JMEPEG (2011) 20:298–305
DOI: 10.1007/s11665-010-9675-4

1059-9495/$19.00

Oxidation of Uncoated and Aluminized 9-12% Cr Boiler Steels at 550-650 °C

J. Metsäjoki, E. Huttunen-Saarivirta, and T. Lepistö

(Submitted January 19, 2010; in revised form March 17, 2010)

In this paper, oxidation behavior of 9-12% Cr steels P91 and HCM12A is studied in air and in a mixture of air and water vapor. Comparison is made between these steels in uncoated condition and coated with aluminum diffusion coating by a slurry method. Oxidation tests were carried out at 550, 600, and 650 °C for a discontinued duration of 1000 h; every 250 h the specimens were slowly cooled to room temperature and weighed. SEM + EDS and XRD characterization were performed after 500 and 1000 h. The results showed that oxidation rate of uncoated P91 and HCM12A was significantly higher in the mixture of air and water vapor than in air. Oxidation resistance of the studied materials improved substantially when they were aluminized.

Keywords diffusion coating, HCM12A, oxidation, P91, slurry coating

1. Introduction

There is an urgent need to produce energy with low adverse emissions. Increasing operating temperatures and pressures in power plants improve their efficiency and, thus, help in achieving this goal. Nevertheless, higher temperatures and pressures give rise to increase in the occurrence and rates of corrosion. Biomass is considered as a CO_2 neutral fuel and, therefore, a very attractive source of energy, but it is also known to cause corrosion at lower temperatures than traditional coal combustion. At present, waste incineration has even more potential for efficiency improvement, because it is usually done at even lower temperatures than combustion of biomass, due to very corrosive flue gases (Ref 1). One way to improve corrosion resistance of components in power plants would be to apply highly resistant Ni-based alloys. Often it is, however, a too expensive alternative. A more economical solution would be surface coatings on cheaper materials, like commonly used 9-12% Cr steels, such as P91 and HCM12A.

Numerous oxidation studies (Ref 2-13) have been conducted on 9-12% Cr ferritic-martensitic boiler steels. They have been reported to have good elevated temperature properties, such as lower coefficient of thermal expansion and better thermal conductivity than austenitic steels or Ni-based alloys. Maximum operating temperature of these steels is limited by mechanical properties to 650 °C but, depending on type of fuel used in combustion, corrosion problems may restrict their use to temperatures well below the theoretical maximum (Ref 14-17).

J. Metsäjoki, E. Huttunen-Saarivirta, and **T. Lepistö,** Department of Materials Science, Tampere University of Technology, P.O. Box 589, 33101 Tampere, Finland. Contact e-mails: jarkko.metsajoki@tut.fi and elina.huttunen-saarivirta@tut.fi.

Surface coatings could be the solution for reaching higher operating temperatures without use of expensive materials. Aluminum coatings deposited by pack cementation or slurry method have been studied to some extent (Ref 2-6) and found to be promising. In this study, we have aluminized two 9-12% Cr ferritic-martensitic steels, P91 and HCM12A, using a slurry method with a commercially available slurry. Formed coatings are studied, and their oxidation behavior is compared to that of uncoated steels. Two simple atmospheres were chosen: air and, in order to distinguish the role of water vapor, a mixture of air and water vapor. Temperatures ranged from 550 °C to the theoretical maximum temperature of the steels, 650 °C.

2. Experimental Procedure

Test specimens were taken from steel pipes which were originally supplied by Vallourec and Mannessmann Tubes (P91) and Sumimoto (HCM12A). Chemical compositions of the steels are shown in Table 1. Specimen size was 10 mm by 10 mm by 2 mm. Final grinding of the uncoated specimens was done with 800 grit SiC-paper. For the coating process, the specimens were first ground with 250 grit SiC-paper (Fig. 1a) and then cleaned in ethanol in an ultrasonic bath.

Coatings were deposited using a slurry method in which a slurry is brushed on a substrate, to produce a diffusion coating when heat treated. The slurry was supplied by Indestructible Paint Ltd. (UK), and it is claimed to consist of mixture of xylene isomers and stabilized aluminum powder. According to EDS analyses of a green state coating (Fig. 1b), roughly 3 at.% of Si has been used in stabilizing the aluminum powder. Three layers of the slurry was brushed on the specimens, let to dry and then heat treated for 10 h at 700 °C under an argon flow. The specimens were cooled to room temperature with the furnace. A layer of loose unreacted slurry was carefully removed by brushing before the tests and the specimens were further cleaned in an ultrasonic bath in ethanol, dried and weighed (Fig. 1c).

Discontinuous oxidation tests of 1000 h were carried out in air and in a mixture of air and 10 vol.% H_2O with a flow rate of

Table 1 Chemical compositions (in wt.%) of the steels

Alloy	Fe	Cr	Mn	Mo	Si	Ni	V	W	Cu
P91	88.2	9.2	0.50	0.90	0.40	0.38	0.22	<0.005	
HCM12A	83.5	12.5	0.54	0.36	0.25	0.34	0.21	1.9	0.85
Alloy	**C**	**Nb**	**N**	**Ti**	**P**	**S**	**Al**	**Co**	**B**
P91	0.089	0.062	0.0489	0.006	0.013	<0.001	0.010	0.008	
HCM12A	0.071	0.045	0.0569		<0.01	<0.001	0.012		<0.005

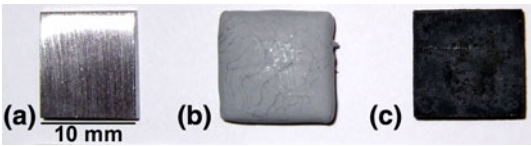

Fig. 1 Slurry aluminizing process. (a) Ground specimen. (b) Dried slurry on a specimen (*green state*). (c) Aluminized specimen after heat treatment and removal of the loose coating

1.5 L/min at temperatures of 550, 600, and 650 °C. Under all conditions, except at 600 °C with water vapor, two identical specimens were exposed to enable microstructural examinations after 500 and 1000 h of exposure. During the tests, the specimens were slowly cooled to room temperature every 250 h for weighing. Weight gain was used to evaluate the oxidation rate of the specimens.

Specimen characterization was done using Philips XL 30 scanning electron microscope (SEM) with an EDAX energy dispersive spectrometer (EDS) and Siemens D500 x-ray diffractometer (XRD) with Cu Kα radiation. To study cross sections, the specimens were sputtered with gold to ensure electric conductivity, coated electrolytically with nickel and mounted to resin to protect the oxide scales during cutting, grinding, and polishing. The nickel coating also provides an excellent contrast between the specimen and the mounting when using back-scattered electrons in SEM investigations.

3. Results and Discussion

3.1 Unexposed Aluminized Specimens

Surface morphology of the aluminized coating was similar on both steels: quite rough (Fig. 2a), slightly layered (Fig. 2b) and relatively dense. However, locally on the top of the dense layer, there appeared also a porous surface layer that was only mechanically attached to the dense layer underneath. When studied with EDS, the porous surface layer consisted mainly of aluminum, which suggests that it was primarily sintered slurry. Small cracks were observed on the dense areas of the coating. Most likely, the cracks appeared during cooling because of thermal expansion mismatch between the coating and the substrate (Ref 3).

Presence of the Al_5Fe_2, $AlCr_2$, and Cr_3Si phases in the coating was confirmed by XRD (Fig. 3). Cross-sectional SEM + EDS studies (Fig. 4) disclosed distribution of the phases (Fig. 5). The $AlCr_2$ and Cr_3Si phases, the latter of which may be detected as brighter of the two in BSE images, appeared as small precipitates in the Al_5Fe_2 phase matrix. A layer of phase with the composition close to the stoichiometric

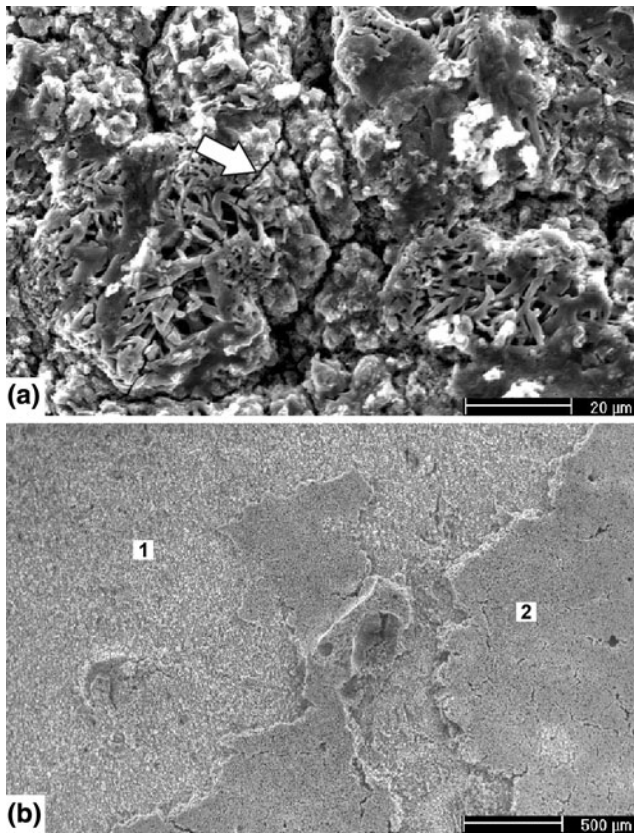

Fig. 2 Secondary electron images showing the surfaces of unexposed aluminized specimens. (a) P91. A small crack is indicated with an *arrow*. (b) HCM12A. (1) Dense coating layer. (2) Porous surface layer on top of the dense layer

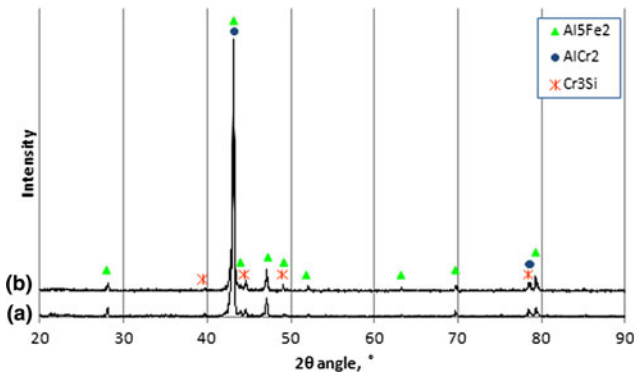

Fig. 3 XRD spectra for unexposed aluminized specimens. (a) P91. (b) HCM12A

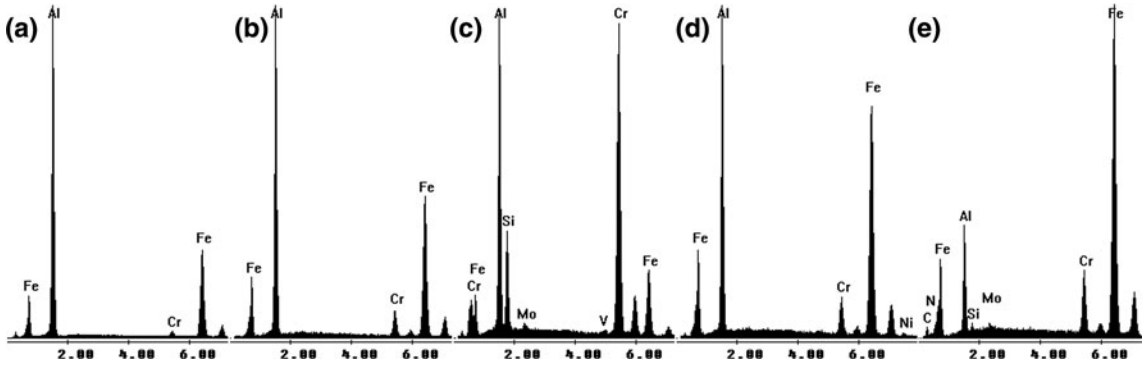

Fig. 4 EDS analyses for a cross section of unexposed aluminized P91 (Fig. 5a). All compositions are given in at.%. (a) Al_5Fe_2 (70.6% Al, 28.2% Fe, 1.2% Cr). (b) $AlCr_2$ (60.4% Al, 35.2% Fe, 4.4% Cr). (c) Cr_3Si (38.3% Al, 37.6% Cr, 12.3% Si, 11.2% Fe, 0.4% Mo, 0.3% V). (d) AlFe (50.2% Al, 44.5% Fe, 4.5% Cr, 0.8% Ni). (e) AlN precipitates (65.0% Fe, 20.7% Al, 7.9% Cr, 5.0% N, 1.0% Si, 0.3% Mo)

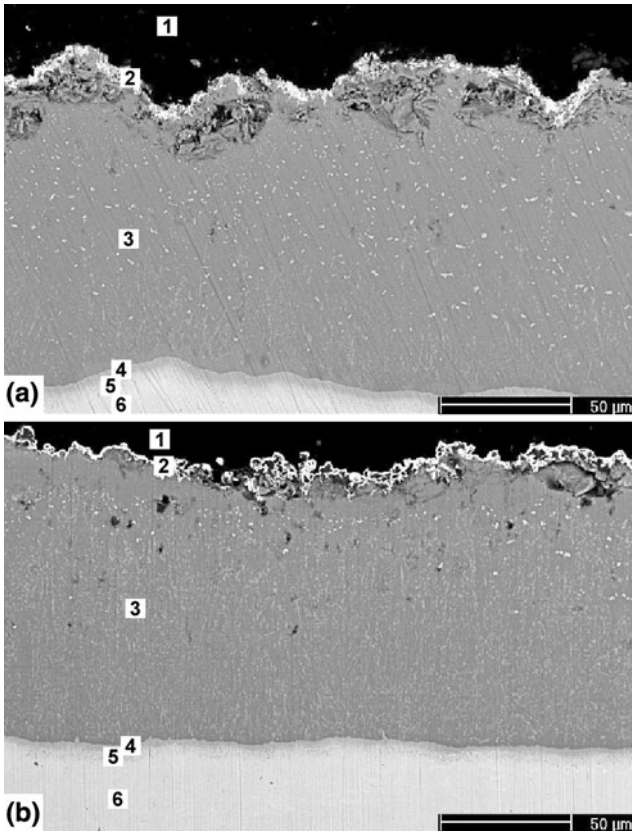

Fig. 5 Back-scattered electron images showing cross sections of unexposed aluminized specimens. (a) P91. (b) HCM12A. On both images: (1) Mounting. (2) Nickel coating. (3) Al_5Fe_2 matrix phase (as *gray* in images) with $AlCr_2$ and Cr_3Si precipitate phases (as *white* in images, the latter shows *brighter*). (4) AlFe phase. (5) AlN precipitates. (6) Substrate

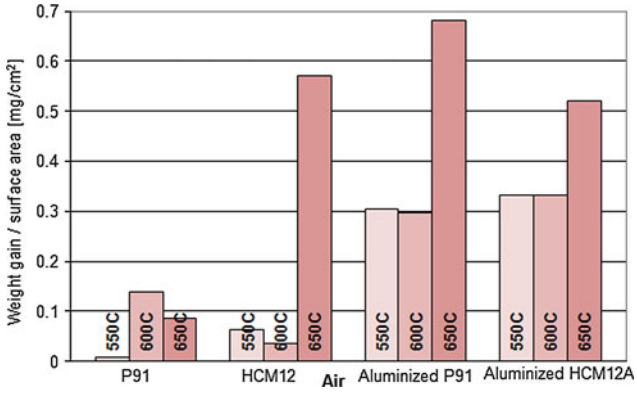

Fig. 6 Relative weight gains for specimens exposed in air for 1000 h

AlFe was found underneath the Al_5Fe_2 phase layer and, finally, the AlN precipitates were detected embedded in the substrate near the coating interface. The findings are supported by previous studies (Ref 2, 6).

3.2 Exposure in Air

In general, weight gains for uncoated specimens exposed in air were low (Fig. 6). In most cases, weight gains remained well below 0.15 mg/cm^2. Thin Cr-rich oxide scales formed on uncoated specimens exposed to air, except for on HCM12A at 650 °C (Fig. 7a) where a thicker Cr-rich oxide scale developed with some evident internal oxidation (Fig. 7b). Due to the thicker scale, the specimen gained more weight than the other uncoated specimens. In each case, the Cr-rich scales were identified by XRD (Fig. 8) to contain Cr_2O_3 or $(Fe, Cr)_2O_3$ with a high Cr content. In addition, Fe_3O_4 was detected in the scales formed at the highest temperature. Although compositionally identical, the oxide scales that formed on the two steels were different in structure and color. On P91, the oxide scale was very fine grained (Fig. 9a) and of a light blue color, whereas, on HCM12A, the scale consisted of large crystals (Fig. 9b) which grew larger with increase in temperature and exposure time and was of a black color.

Weight gains for aluminized specimens were higher than for the uncoated specimens; typically the gains were about 0.3 mg/cm^2 or more. The most likely explanation for this is a rough coating surface: they had more active surface area than the ground uncoated specimens. In the case of the aluminized specimens exposed in the two lowest temperatures, similar oxidation of the specimens was typically detected in SEM examinations. However, the exposed aluminized specimens experienced significantly more charging under the electron beam of SEM, especially the Al-rich surface layers (Fig. 10a), than the unexposed specimens which suggest a decrease in conductivity, apparently because of oxidation. Specimens

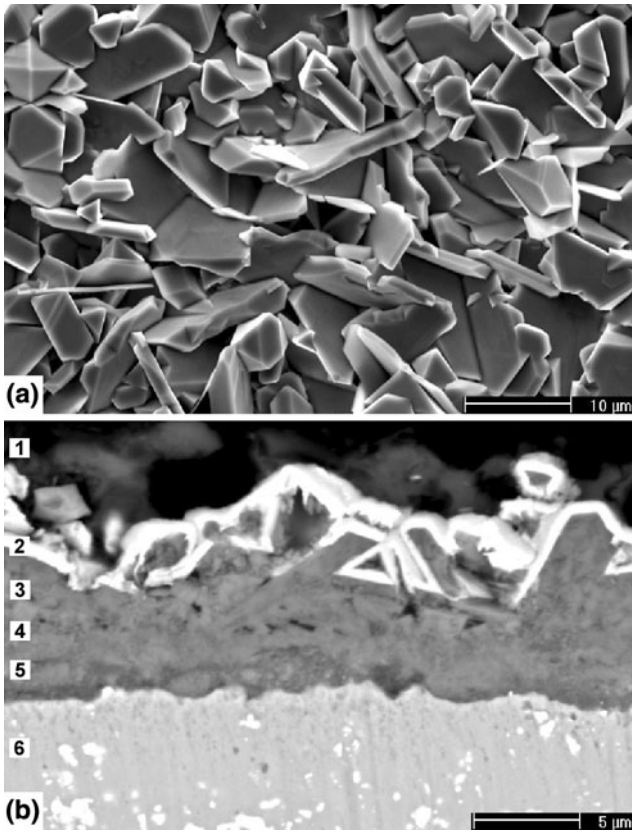

Fig. 7 (a) Secondary electron image showing the surface of uncoated HCM12A after 1000 h at 650 °C in air. (b) Back-scattered electron image showing cross section of the uncoated HCM12A exposed at 650 °C for 1000 h in air. (1) Mounting. (2) Nickel coating. (3) Cr-rich oxide scale. (4) Original surface. (5) Internal oxidation. (6) Substrate

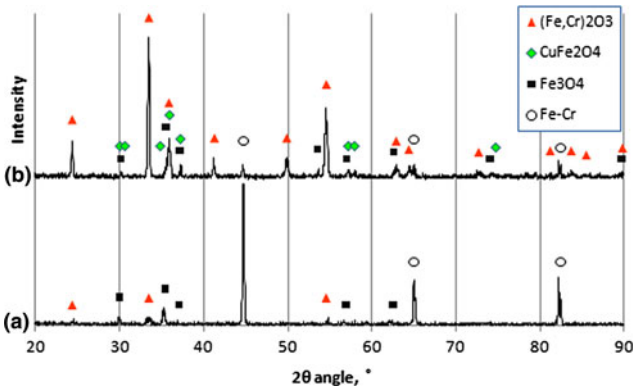

Fig. 8 XRD spectra for uncoated specimens exposed for 1000 h at 650 °C in air. (a) P91 and (b) HCM12A

exposed at the highest temperature showed more evidence (Fig. 11) for oxide scale growth, as also suggested by the weight gain data shown in Fig. 5. Small amounts of the γ-Al_2O_3 were identified by XRD (Fig. 12) on all aluminized specimens after exposure of 1000 h. Small cracks, similar to those seen after aluminizing, were also observed on both aluminized steels after the exposure in air (Fig. 10b).

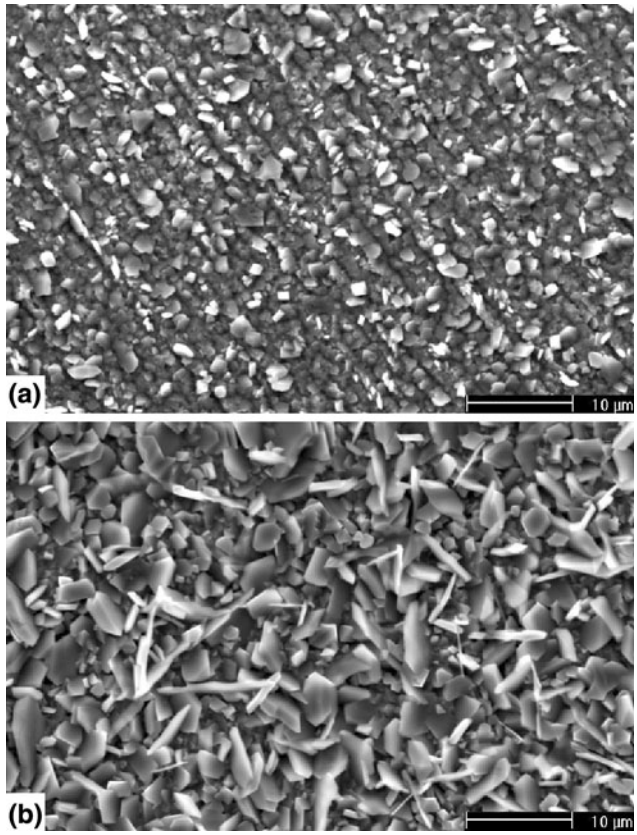

Fig. 9 Secondary electron images showing the surfaces of uncoated specimens after 1000 h at 600 °C in air. (a) P91. (b) HCM12A

Cross-sectional SEM studies of the aluminized specimens (Fig. 13) showed that the cracks which were observed on the surface do not expose the substrate to oxidation. Oxygen was only detected at the surface of the coating and, hence, the growth of γ-Al_2O_3 was limited to the surface of the coating. The cross-sectional studies also indicated diffusion within the specimens, with significant differences being observed between the exposure temperatures and the substrate used. After exposure at 550 °C, the cross sections were very similar to that of the unexposed specimens, apparently because the temperature was too low for any significant diffusion to occur during exposure, but after exposure at 600 °C, there were clear signs of diffusion, such as thickening of AlFe layer, and even more so after exposure at 650 °C. Diffusion can also lead to Kirkendall porosity at the coating-substrate interface and cause spallation of the coating before Al-content of the surface falls below protective level (Ref 2).

3.3 Exposure in Air: 10 Vol.% H_2O

Uncoated specimens exposed to a mixture of air and water vapor experienced significant weight gains compared to the dry atmosphere even at the lowest exposure temperature of 550 °C (Fig. 14a). Weight gain average of all uncoated specimens at air was 0.1 mg/cm^2, while in the mixture of air and water vapor the average rose to 6 mg/cm^2. In the presence of water vapor, formed oxide scales were thick, porous and, in the case of P91 at the two highest temperatures, prone to spallation (Fig. 15a). Some of the spalled scale was lost during the tests which lowered the weight gains of the specimens. In Fig. 14(b), it can

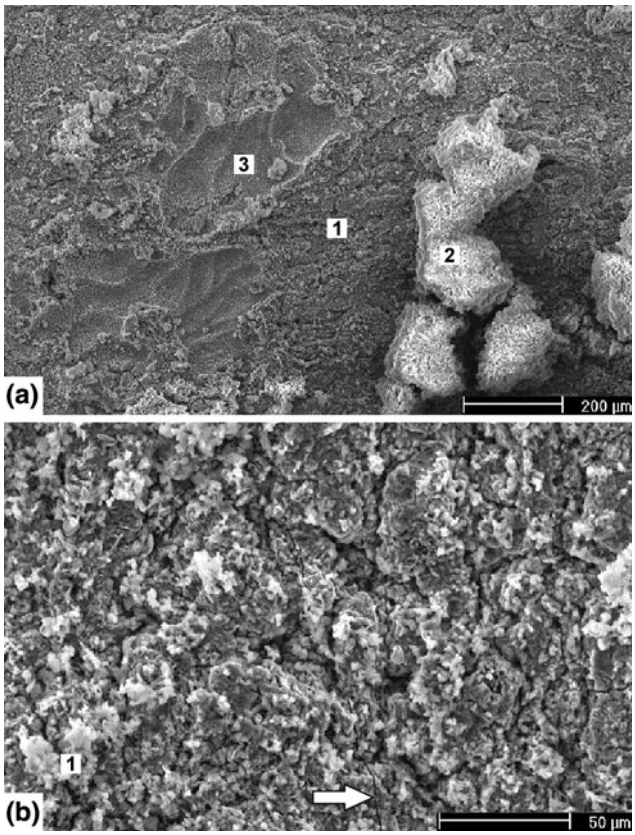

Fig. 10 Secondary electron images showing the surfaces of aluminized specimens after 1000 h at 600 °C in air. (a) P91. (1) Oxidized dense coating layer. (2) Probably oxidized porous Al-rich surface layer on top of the dense layer. (3) A pit, left behind by the removal of the porous outer layer. (b) HCM12A. A small crack is indicated with an *arrow*. (1) Alumina growth on the dense coating

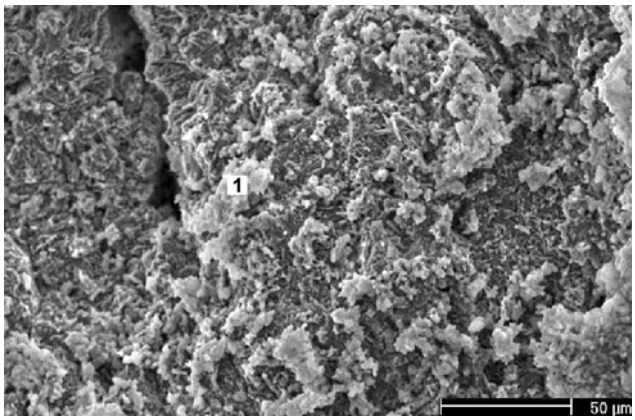

Fig. 11 Secondary electron image showing the surface of aluminized P91 after 1000 h at 650 °C in air. (1) Alumina growth on the surface

be seen that, at 600 and 650 °C, uncoated HCM12A experienced relatively low weight gains at the beginning of the tests, but relatively much greater gains at the later stages of the test. Similar behavior has been previously reported on 12% Cr steels (Ref 11) and is caused by a faster diffusion of Cr to the scale at higher temperatures, giving a protective chromia (Cr_2O_3) scale.

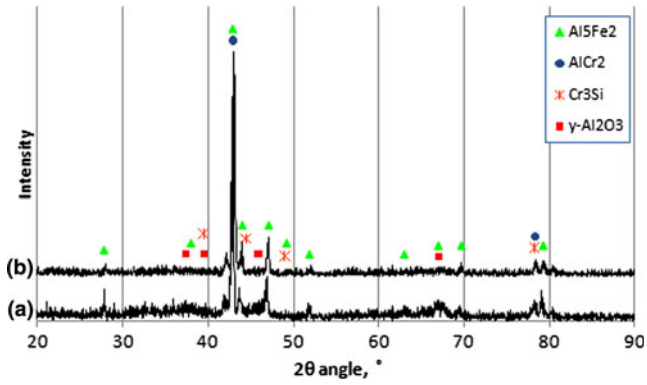

Fig. 12 XRD spectra for aluminized specimens exposed for 1000 h at 650 °C in air. (a) P91. (b) HCM12A

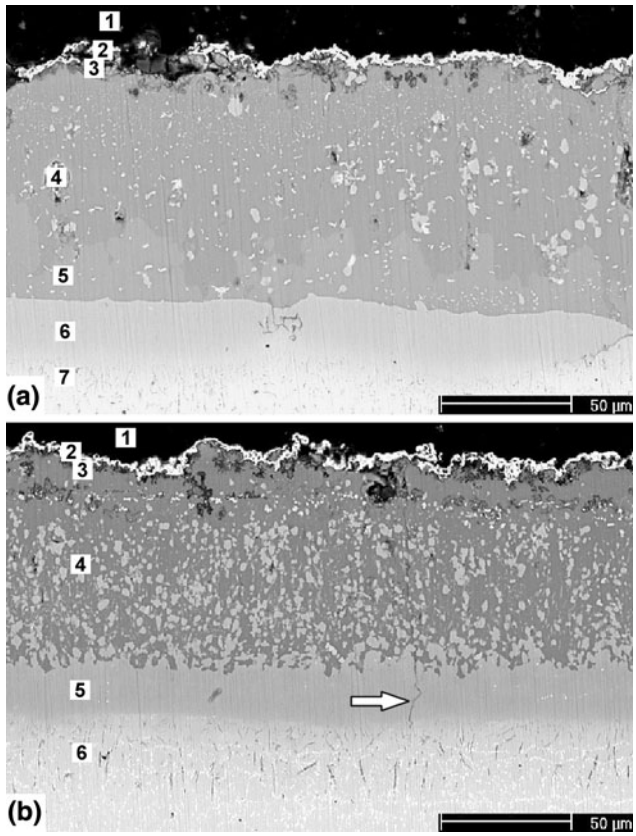

Fig. 13 Back-scattered electron images showing cross sections of aluminized specimens after 1000 h at 650 °C in air. (a) P91. (1) Mounting. (2) Ni-coating. (3) γ-Al_2O_3. (4) Al_5Fe_2 phase matrix with $AlCr_2$ and Cr_3Si phases. (5) A phase with intermediate Fe concentration to Al_5Fe_2 and AlFe. (6) AlFe phase. (7) AlN precipitates. (b) HCM12A. (1) Mounting. (2) Ni-coating. (3) γ-Al_2O_3. (4) Al_5Fe_2 phase matrix with AlFe. (5) AlFe phase. (6) AlN precipitates

However, eventually the protectivity of the scale fails and oxidation rate increases (Ref 4, 7, 11, 18).

Aluminized specimens exposed to the mixture of air and water vapor had similar oxidation behavior than in the dry atmosphere: only very little oxidation was observed at the two lowest temperatures, but somewhat more oxidation at the highest temperature. Weight gains were only slightly higher than in air, probably because of slightly thicker oxide scales.

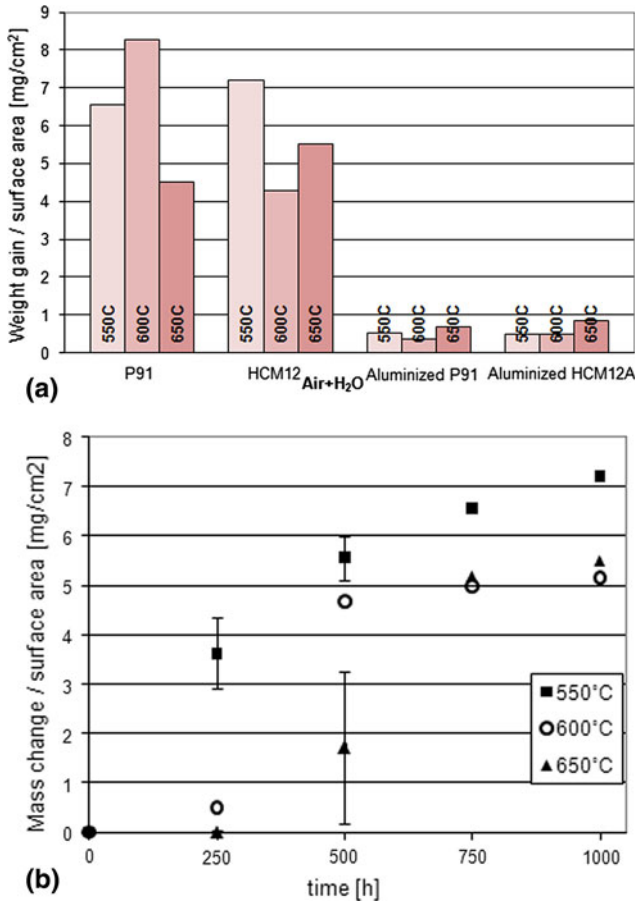

Fig. 14 Relative weight gains for specimens in air-10 vol.% H_2O. (a) For all studied materials after 1000 h. (b) For uncoated HCM12A as function of exposure time. The error bars in some of the measuring points are due to two parallel specimens that were exposed for the first 500 h

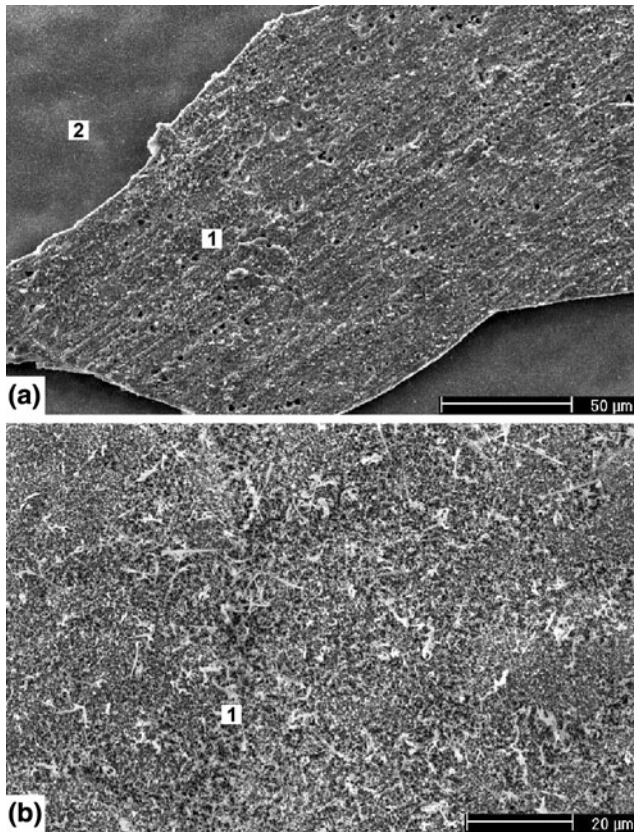

Fig. 15 Secondary electron images showing the surfaces of uncoated specimens after 1000 h exposure in air-10 vol.% H_2O at 600 °C. (a) P91. (1) A porous layer of oxide. (2) Spalled area of the scale. (b) HCM12A. (1) Cu containing ridges on the oxide scale

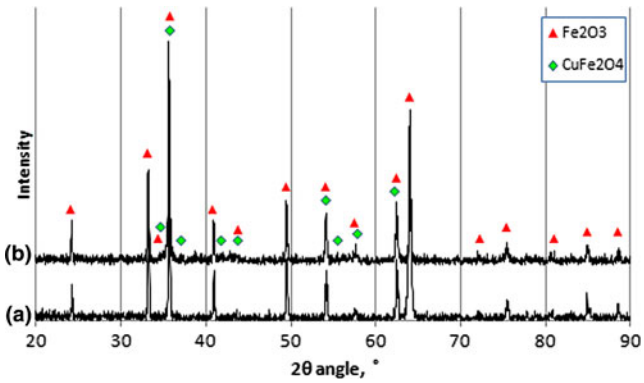

Fig. 16 XRD spectra for uncoated specimens exposed for 1000 h at 600 °C in air-10% water vapor. (a) P91 and (b) HCM12A

In general, the water vapor did not seem to change oxidation behavior of aluminized P91 and HCM12A in air.

As mentioned above, thick and porous oxide scales formed on the uncoated specimens, both on P91 and HCM12A, at all temperatures. On P91, the scales experienced spallation. Figure 15(a) shows that the surface of the outermost layer of the scale which, occasionally spalled of, had pits and was rougher than the oxide layer revealed underneath. On HCM12A (Fig. 15b), a network of ridges appeared at all temperatures on the specimen surface. Cr was not found in the surface of the oxide scales that formed on P91 and HCM12A. XRD studies (Fig. 16a) indicated the surfaces of all uncoated P91 specimens to consist of hematite (Fe_2O_3). On all uncoated HCM12A specimens, in addition to hematite, small amounts of $CuFe_2O_4$ were identified (Fig. 16b). With SEM + EDS, Cu was mainly found in the ridges on the oxide scale (Fig. 15b). On the aluminized specimens, a small amount of γ-Al_2O_3 was detected by XRD (Fig. 17).

Cross-sectional SEM studies of the uncoated specimens (Fig. 18) revealed that the oxide scales on both P91 and HCM12A had a layered structure, in which the original surface is a dividing line between a porous outer layer and a denser Cr-rich inner layer. Cu which was found in ridges on surface of HCM12A, was only enriched on top of the scale. It is worth mentioning that copper is added in HCM12A to suppress the formation of δ-ferrite and to allow higher Cr content in the alloy (Ref 19).

Apart from Cu, the outer layers of oxide scales formed on both steels were similar in structure and composition. In the inner layer of the scales, below the original surface, more Cr was found in HCM12A than in P91, which was expected, based on the compositions of the steels. HCM12A also has W alloying which is detected in light precipitates, seen in back-scattered electron images taken with SEM (Fig. 18b).

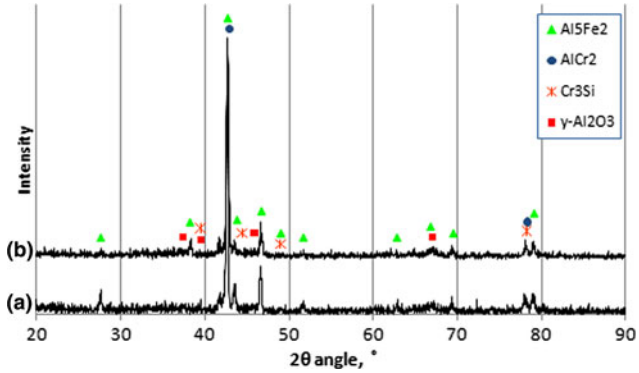

Fig. 17 XRD spectra for aluminized specimens exposed for 1000 h at 600 °C in air-10% water vapor. (a) P91 and (b) HCM12A

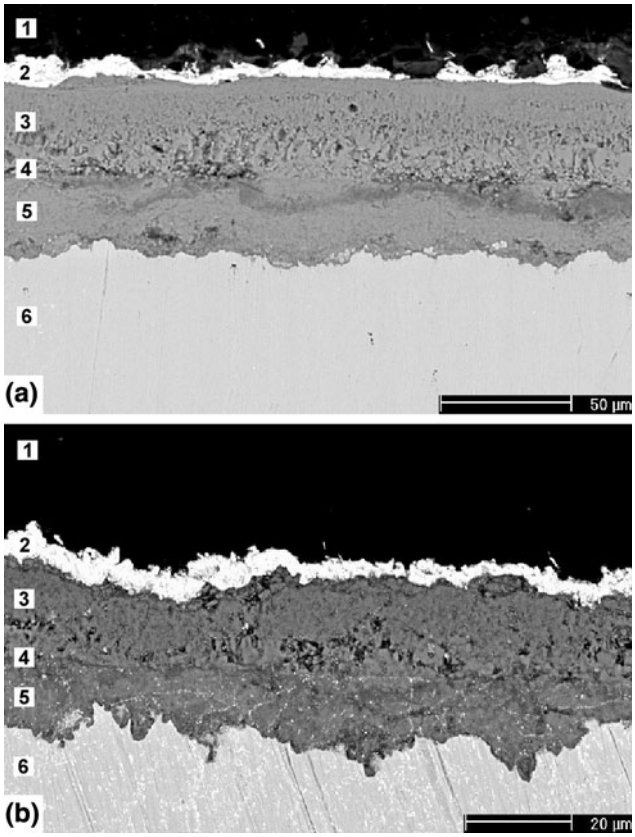

Fig. 18 Back-scattered electron images showing cross sections of uncoated specimens after 1000 h exposure in air-10 vol.% H_2O at 600 °C. (a) P91. (b) HCM12A. On both pictures: (1) Mounting. (2) Ni-coating. (3) Outer oxide layer. (4) Original surface. (5) Inner oxide layer. (6) Substrate

The W-rich precipitates were present in the steel and also in the inner oxide scale, maybe in an oxidized form, which supports the claim that the dividing line between inner and outer scale was the original surface of the specimen.

Under all conditions, cross-sectional SEM studies of the aluminized specimens revealed no differences between the test atmospheres. The γ-Al_2O_3 only existed on the surface, cracks did not expose the substrate and diffusion proceeded like it did in dry air atmosphere. Overall, the results of this study show that oxidation of Cr-containing steels P91 and HCM12A introduces scales, where $(Fe,Cr)_2O_3$, Fe_2O_3, and Fe_3O_4 are detected on top of the substrate. This is in agreement with literature (Ref 20). The results also indicate that oxidation of aluminized specimens follows the theoretical approach, because the γ-Al_2O_3 forms on the surface. This is the "low-temperature" Al_2O_3 that often develops on Al-rich surfaces below 900 °C (Ref 21). As the rate of oxide scale development on the aluminized surface is evidently much lower than on the Cr-Fe substrate, the aluminized layer provides protection to the substrate against oxidation, particularly in water-vapor-containing air. Tests in more aggressive atmospheres are conducted at present.

4. Conclusions

The results showed that oxidation behavior of uncoated 9-12% Cr steels P91 and HCM12A was significantly different in air and in the mixture of air and water vapor, at temperatures of 550, 600, and 650 °C. In exposure in air, thin and protective Cr-rich oxide scales formed on both steels in most cases, but, when exposed to a mixture of air and 10 vol.% water vapor, the scales were thick, layered, porous and, in case of P91, prone to spallation. The different thicknesses of the scales formed in different atmospheres were also evident in weight gain data: weight gains were significantly higher in a water-vapor-containing atmosphere.

Aluminized specimens were not significantly affected by the presence of water vapor in air. The only notable difference between the atmospheres was slightly higher weight gains in a mixture of air and water vapor compared to those in air; this was probably due to slightly thicker oxide scales. When compared to uncoated specimens exposed to a mixture of air and water vapor, weight gains of the aluminized specimens were significantly lower. Based on these results, aluminizing shows great prospect in protecting steels in water-vapor-containing atmospheres encountered in many combustion processes.

Acknowledgment

The authors thank the Academy of Finland (decision 111948) for financial support.

References

1. K. Salmenoja and K. Mäkelä, Prevention of Superheater Corrosion in the Combustion of Biofuels, *Corrosion 2000*, March 26-31, 2000 (Orlando, Fl, USA), NACE, paper 00238
2. A. Agüero, R. Muelas, M. Gutiérrez, R. Van Vulpen, S. Osgerby, and J.P. Banks, Cyclic Oxidation and Mechanical Behaviour of Slurry Aluminide Coatings for Steam Turbine Components, *Surf. Coat. Technol.*, 2007, **201**(14), p 6253–6260
3. A. Agüero, R. Muelas, A. Pastor, and S. Osgerby, Long Exposure Steam Oxidation Testing and Mechanical Properties of Slurry Aluminide Coatings for Steam Turbine Components, *Surf Coat. Technol.*, 2005, **200**(5–6), p 1219–1224
4. F.J. Pérez and S.I. Castañeda, Study of Oxyhydroxides Formation on P91 Ferritic Steel and Slurry Coated by Al in Contact With Ar + 80% H_2O at 650°C by TG-Mass Spectrometry, *Surf. Coat. Technol.*, 2007, **201**(14), p 6239–6246

5. V. Rohr, A. Donchev, M. Schütze, A. Milewska, and F.J. Pérez, Diffusion Coatings for High Temperature Corrosion Protection of 9-12%Cr Steels, *Corros. Eng. Sci. Technol.*, 2005, **40**(3), p 226–232
6. E. Huttunen-Saarivirta, F.H. Stott, V. Rohr, and M. Schütze, Erosion-Oxidation Behaviour of Pack-Aluminized 9% Chromium Steel Under Fluidized-Bed Conditions at Elevated Temperature, *Corros. Sci.*, 2007, **49**(7), p 2844–2865
7. M. Schütze, M. Schorr, D.P. Renusch, A. Donchev, and J.P.T. Vossen, The Role of Alloy Composition, Environment and Stresses for the Oxidation Resistance of Modern 9% Cr Steels for Fossil Power Stations, *Mater. Res.*, 2004, **7**(1), p 111–123
8. H. Nickel, Y. Wouters, M. Thiele, and W.J. Quadakkers, The Effect of Water Vapor on the Oxidation Behavior of 9%Cr Steels in Simulated Combustion Gases, *Fresenius J. Anal. Chem.*, 1998, **361**(6–7), p 540–544
9. P.J. Ennis and W.J. Quadakkers, Mechanisms of Steam Oxidation in High Strength Martensitic Steels, *Int. J. Press Vessel Pip.*, 2007, **84**(1–2), p 75–81
10. J. Ehlers, D.J. Young, E.J. Smaardijk, A.K. Tyagi, H.J. Penkalla, L. Singheiser, and W.J. Quadakkers, Enhanced Oxidation of the 9% Cr Steel P91 in Water Vapour Containing Environments, *Corros. Sci.*, 2006, **48**(11), p 3428–3454
11. J. Zurek, E. Wessel, L. Niewolak, F. Schmitz, T.-U. Kern, L. Singheiser, and W.J. Quadakkers, Anomalous Temperature Dependence of Oxidation Kinetics During Steam Oxidation of Ferritic Steels in the Temperature Range 550-650°C, *Corros. Sci.*, 2004, **46**(9), p 2301–2317
12. J. Zurek, M. Michalik, F. Schmitz, T.-U. Kern, L. Singheiser, and W.J. Quadakkers, The Effect of Water-Vapor Content and Gas Flow Rate on the Oxidation Mechanism of a 10%Cr-Ferritic Steel in Ar-H2O Mixtures, *Oxid. Met.*, 2005, **63**(5–6), p 401–422
13. M. Schütze, D. Renusch, and M. Schorr, Parameters Determining the Breakaway Oxidation Behaviour of Ferritic Martensitic 9%Cr Steels in Environments Containing H_2O, *Corros. Eng. Sci. Technol.*, 2004, **39**(2), p 157–166
14. R. Viswanathan and W.T. Bakker, Materials for Boilers in Ultra Supercritical Power Plants, *Proceedings of International Joint Power Generation Conference 2000* (Miami Beach, Fl, USA), 2000, paper 15049
15. R. Viswanathan, Materials Technology for Coal-Fired Power Plants, *Adv. Mater. Process.*, 2004, **162**(8), p 73–76
16. H.P. Nielsen, F.J. Frandsen, K. Dam-Johansen, and L.L. Baxter, The Implications of Chlorine Associated Corrosion on the Operation of Biomass-Fired Boilers, *Prog. Energy Combust. Sci.*, 2000, **26**(3), p 283–298
17. M. Noguchi, H. Yakuwa, M. Miyasaka, M. Yokono, A. Matsumoto, K. Miyoshi, K. Kosaka, and Y. Fukuda, Experience of Superheater Tubes in Municipal Waste Incineration Plant, *Mater. Corros.*, 2000, **51**(11), p 774–785
18. L. Nieto Hierro, V. Rohr, P.J. Ennis, M. Schütze, and W.J. Quadakkers, Steam Oxidation and Its Potential Effects on Creep Strength of Power Station Materials, *Mater. Corros.*, 2005, **56**(12), p 890–896
19. M. Hättestrand, M. Schwind, and H.-O. Andrén, Microanalysis of Two Creep Resistant 9-12% Chromium Steels, *Mater. Sci. Eng. A*, 1998, **250**(1), p 27–36
20. M. Schütze, *Protective Oxide Scales and Their Breakdown*, Institute of Corrosion and Wiley, England, 1997
21. P. Kofstad, *High Temperature Corrosion*, Elsevier Applied Science Publishers Ltd, Essex, England, 1988